

Journal of Materials Chemistry A

Accepted Manuscript



This is an *Accepted Manuscript*, which has been through the Royal Society of Chemistry peer review process and has been accepted for publication.

Accepted Manuscripts are published online shortly after acceptance, before technical editing, formatting and proof reading. Using this free service, authors can make their results available to the community, in citable form, before we publish the edited article. We will replace this *Accepted Manuscript* with the edited and formatted *Advance Article* as soon as it is available.

You can find more information about *Accepted Manuscripts* in the [Information for Authors](#).

Please note that technical editing may introduce minor changes to the text and/or graphics, which may alter content. The journal's standard [Terms & Conditions](#) and the [Ethical guidelines](#) still apply. In no event shall the Royal Society of Chemistry be held responsible for any errors or omissions in this *Accepted Manuscript* or any consequences arising from the use of any information it contains.

ARTICLE

Highly Flexible and Transferable Supercapacitors with Ordered Three-dimensional MnO₂/Au/MnO₂ Nanospikes Arrays

Cite this: DOI: 10.1039/x0xx00000x

Received 00th March 2015,
Accepted 00th March 2015

DOI: 10.1039/x0xx00000x

www.rsc.org/

Yuan Gao,^a Huanyu Jin,^b Qingfeng Lin,^a Xiang Li,^a Mohammad Mahdi Tavakoli,^a Siu-Fung Leung,^a Wing Man Tang,^b Limin Zhou,^c Helen Lai Wa Chan,^b Zhiyong Fan^{*a}

Ordered three-dimensional nanostructures are highly attractive for energy storage application, particularly for high-performance flexible supercapacitors. Here, we report a unique MnO₂/Au/MnO₂ Nanospikes (MAMNSPs) supercapacitor structure based on free-standing 3-D gold (Au) NSPs film. The NSPs films are highly flexible and transferable to arbitrary type of flexible substrate to enable applications that require high flexibility. The large surface area of this unique structure leads remarkable enhancement in electrochemical performance, 1.9 and 4.26 times capacitance as compared with MnO₂/Au NSPs (MANSPs) and MnO₂/Planar (MAPL) electrodes, respectively. The all-solid-state symmetric supercapacitors based on MAMNSPs electrodes have been fabricated and systematic performance characterizations showed that the devices have high volumetric capacitance of 20.35 F cm⁻³ and specific energy of 1.75 × 10⁻³ Wh cm⁻³. In addition, bendability measurement showed that the supercapacitor devices are highly flexible and reliable. With virtue of simple fabrication procedures and enhanced electrochemical performance, such 3-D structures have highly promising potency for portable and flexible energy storage systems for a wide range of practical applications.

Introduction

Three-dimensional nanostructures, such as arrays of nanowires (NWs), nanopillars (NPLs), nanospikes (NSPs), nanocones (NCNs), etc., naturally have large surface/interface area which can be harnessed for applications that are sensitive to surface processes, such as chemical/biological sensing,^{1,2} surface catalysis,^{3,4} as well as energy generation^{5,6} and storage.^{7,8} Particularly for energy storage, primarily these nanostructures have been used for supercapacitors and batteries.^{9,10} As compared with battery, supercapacitors have appealing attributes including fast charging/discharging rate, more safe operation and long cycle lifetime thus they have triggered enormous research interest.¹¹⁻¹⁴ It is worth noting that due to the fast growth of portable electronics market, reliable, light weight and flexible energy storage devices are in urgent demand. Therefore, extensive research has been carried out on nanostructure based flexible supercapacitors.¹⁵⁻²⁵ In fact, in most of the existing works, the nanostructures have relatively thick supporting substrates, or the structures themselves have thickness of

tens of micrometers to millimeters. Thus their bendability/flexibility has a constraint.^{16,26,27} Herein, we report a unique supercapacitor structure based on ultra-thin, free-standing 3-D gold (Au) NSPs film. The NSPs films are highly flexible and transferable to arbitrary type of flexible substrate to enable applications that require high flexibility. The large surface area of NSPs is utilized to achieve respectable pseudocapacitance together with thin layer of MnO₂ coating. The all-solid-state symmetric supercapacitors based on MnO₂/Au/MnO₂ NSPs (MAMNSPs) electrodes have been fabricated in this work and systematic performance characterizations showed that the devices have volumetric capacitance of 20.35 F cm⁻³ and the highest specific energy and specific power of 1.75 × 10⁻³ Wh cm⁻³ and 13.46 W cm⁻³, respectively. Furthermore, bendability measurement showed that the supercapacitor devices are highly flexible and reliable. They are operational even with 180 degree bending angle and they can preserve 88 % capacitance after 5,000 cycled bending. These results have shown that the flexible NSPs electrodes are highly promising for high performance and flexible supercapacitor devices.

Results and discussion

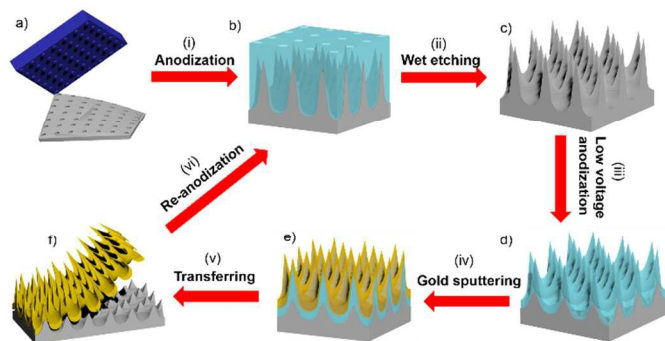


Figure 1 Schematic illustration showing the fabrication process of free-standing Au NSPs film. **a)** Nanoimprint process with a square ordered nanopillars Si mold. **b)** Aluminum oxide achieved by anodization. **c)** As-prepared Al NSPs template. **d)** Alumina NSPs achieved by low voltage anodization. **e)** 100 nm Au-coated alumina NSPs. **f)** Free-standing Au NSPs film after etching away sacrificial alumina layer.

The free-standing Au NSPs film fabrication process mainly comprises six steps shown in Figure 1: i) Nanoimprint assisted electrochemical preparation of a template with aluminum (Al) NSPs (Figure 1a and b). This process was previously developed by us for nanostructured solar cells;⁵ ii) Wet etching of anodized aluminum oxide to achieve pure Al NSPs (Figure 1c); iii) Low voltage anodization on the Al NSP substrates to achieve a thin sacrificial layer of alumina (light blue color layer in Figure 1d) on NSPs; iv) Sputtering of a 100 nm and highly conductive Au layer on alumina NSPs (Figure 1e); v) Etching away the sacrificial alumina layer and transfer of the Au NSPs film onto an arbitrary flexible substrate; vi) Re-anodization of the patterned substrate to form NSPs again. It is worth pointing out that in this fabrication scheme, the substrate is reusable for many cycles and only one time nanoimprint is required, thus greatly reduced the process cost and complexity.

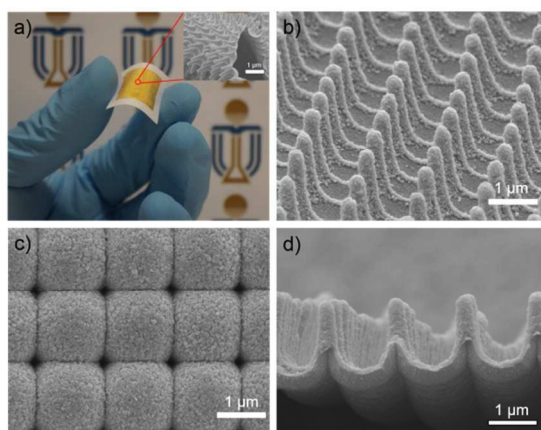


Figure 2 **a)** Photographs of free-standing Au NSPs film transferred onto regular Xerox printing paper and SEM image (insert) shows the microstructure upon bending. **b-d)** SEM images of as-prepared MAMNSPs electrode, **b)** top view, **c)** back view and **d)** side view.

Figure 2a shows a photograph of the Au NSPs film transferred to a piece regular Xerox printing paper demonstrating its appealing flexibility, and the inset scanning electron microscopy (SEM) image shows the microstructure of a free-standing NSPs electrode upon

bending. Interestingly, it is discovered in our work that the NSPs electrode film is quite robust. As shown in Supplementary Information (SI, Figure S1), the film can be directly picked up from an aqueous solution with tweezers. Upon leaving the surface of the solution, the film wraps itself up to form a roll due to water surface tension. And when the roll of the film is placed back to the solution, the film unwraps itself naturally without any observable wrinkles and cracks. Unlike 2-D films consists of metal nanowire network, which need package material to maintain the robustness,²⁸ this interesting behavior of unique structure can be rationalized by considering i) relative inert surface of Au itself, ii) excellent flexibility of 100 nm Au film and most importantly iii) NSP structure leads to point contact between the NSPs and the backside of Au film when it forms a roll, thus leading to much lower bonding energy in the roll, as schematically shown in SI, Figure S1g. The excellent flexibility and transferability render the Au NSPs film compatibility to various types of substrates. Besides the paper substrates shown in Figure 2a, polycarbonate (PC) plastic substrate can also serve as the holding substrate for the Au NSPs film (SI, Figure S2a).

In the past, we have discovered that the geometric factors of the NSPs, including pitch and height can be precisely engineered.^{5, 29} For photovoltaic applications, there exists an intermediate and optimal aspect ratio arose from the balanced design considering both optical light trapping and photovoltaic thin film deposition uniformity. While for applications such as supercapacitors, naturally large surface area is preferred. To obtain an optimized structure with the highest surface area, Au NSPs film with different pitches, including 0.5 μm , 1 μm , 1.2 μm , and 1.5 μm were fabricated (SI, Figure S3a-d). It was measured that the heights of NSPs arrays according to these pitches are 0.42 μm , 0.98 μm , 1.22 μm , and 1.57 μm , respectively. In order to identify the structure with the largest surface area, surface area calculation was performed using the structural schematic (SI, Figure S4a). As the result, it was found that NSPs with the pitches of 1 μm , 1.2 μm , and 1.5 μm have fair close surface area which is nearly 3.3 times that of the area of a flat planar electrode with the same project area (SI, Figure S4b). Considering the fact that larger pitch is preferable for more uniform Au film sputtering, 1.5 μm pitch NSPs films were chosen for the subsequent device fabrication, and such films can be fabricated as large as 1.5 cm \times 1.5 cm with excellent uniformity (SI, Figure S2b).

Flexible and transferable Au NSPs film is a preferable structure for flexible supercapacitor device, due to the enlarged surface area. In order to realize NSPs based supercapacitor device, MnO_2 was electrochemically deposited onto the Au NSP film electrode. Since the Xerox paper has certain porosity, MnO_2 was eventually deposited onto both the front side and the back side of the Au NSPs film forming MAMNSPs configuration. This unique feature leads to more efficient utilization of NSPs film surface area. Due to the conformal nature of the electrodeposition, NSPs shape can be well preserved after electrodeposition of 40 nm MnO_2 layers. Figure 2b shows the tilted angle view SEM of the front side of a MnO_2 coated NSP array with the conformality clearly demonstrated. Figure 2c shows the dome-like structure at the back side of the NSPs film and the cavities at the corners of the domes can be resolved. These cavities are the results of etching away of alumina NSPs (Figure 1c), and they provide additional large surface area at the back side of NSPs as well. Meanwhile, nanoflake structure can be observed from MnO_2 surface and this nanoflake structure could further increase electrode surface area and promote ion diffusion and expedite electron transfer. The cross sectional SEM image of a MAMNSPs electrode is shown in Figure 2d, the height of NSPs is 1.5 μm and the thickness of MnO_2 nanoflake film is around 40 nm on each side. The detailed chemical composition of MAMNSPs electrode was

probed by X-ray photoelectron spectroscopy (XPS) (SI, Figure S5a and b), two peaks at 641.9 eV and 653.7 eV can be identified, which indicates the Mn⁴⁺ ions are dominant in the product. Wide angle of X-ray diffraction result of as prepared MAMNSPs electrode is also shown in Figure S5c.

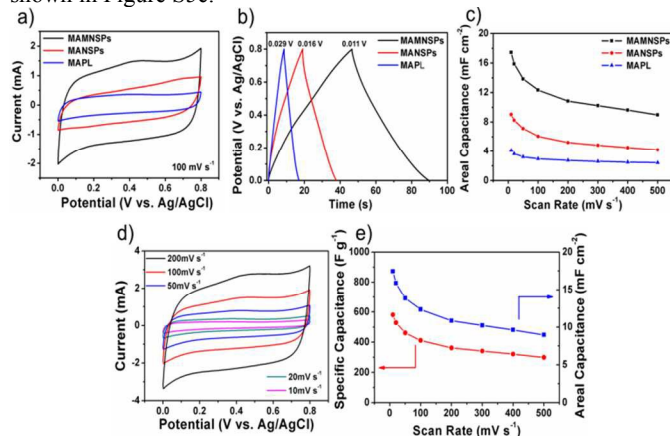


Figure 3 a) CV curves of MAMNSPs, MANSPs and MAPL electrodes at the scan rate of 100 mV s⁻¹ in 1 M aqueous Na₂SO₄ electrolyte. b) GCD curves of MAMNSPs, MANSPs and MAPL electrodes at the same current density (0.3 mA cm⁻²) with different voltage drops. c) Areal capacitance of MAMNSPs, MANSPs, MAPL electrodes as a function of the scan rate. d) CV curves of MAMNSPs electrode at different scan rates (10 mV s⁻¹ - 200 mV s⁻¹). e) Areal and specific capacitance of MAMNSPs at different scan rates.

To evaluate the electrochemical performance of MAMNSPs electrode, cyclic voltammetry (CV) measurements with a three-electrode configuration based on the as-prepared electrode with 0.5 cm × 0.5 cm footprint area was conducted in 1 M Na₂SO₄ liquid electrolyte with voltage ranging from 0 to 0.8 V. Figure 3a presents the typical CV curves at the scan rate of 100 mV s⁻¹ after electrodeposition of MnO₂ on different structures including MAMNSPs, MnO₂/Au NSPs (MANSPs), and MnO₂/Au Planar (MAPL). Note that MANSPs structure refers to the non-transferred Au film deposited on alumina NSPs thus only the front side of the NSP film was deposited with a layer of MnO₂ film, and the MAPL structure is a planar glass sputtered with 100 nm thick Au. In addition, MnO₂ mass loading on these three structures are the same for the sake of a fair comparison. It can be seen from Figure 3a that much more symmetrically rectangular shape and larger area surrounded by CV curve shows MAMNSPs electrode has the best pseudo-capacitive behavior. Galvanostatic charge-discharge (GCD) characteristics based on different architectures are also plotted in Figure 3b. Notably, the lower voltage drop of 0.011 V for MAMNSPs suggests lower internal resistance, which is the result of thinner MnO₂ in MAMNSPs structure since it has the largest area among all three structures with the same MnO₂ mass loading. And the larger area enclosed by charge-discharge curve demonstrates more charge stored in the electrode with the complete redox reaction for the active material on the surface, which can also be attributed to the larger surface area of the electrode for thinner mass loading. The areal capacitance and the specific capacitance are two critical parameters to determine pseudo-capacitive performance of an electrode, which can be calculated by using the following equations:

$$C_s = \int_0^{0.8} (|I_{Au/MnO_2}| - |I_{Au}|) dU / 2m\Delta U v_0 \quad (1)$$

$$C_a = \int_0^{0.8} (|I_{Au/MnO_2}| - |I_{Au}|) dU / 2s\Delta U v_0 \quad (2)$$

$$m = QM / 2eN_A \quad (3)$$

where C_s and C_a are specific capacitance and areal capacitance of the electrode, respectively. m and s are the mass of MnO₂ and the

footprint area of the electrode. I is the electrical current, U is the voltage, ΔU is the operating voltage window (0.8 V), v_0 is the scan rate. Q is the amount of charge passing through the entire electrode, M is the molecular weight of MnO₂, e is the electronic charge, and N_A is the Avogadro's number. As shown in Figure 3c, the areal capacitance for MAMNSPs, MANSPs, and MAPL at the scan rate of 10 mV s⁻¹ is 17.44 mF cm⁻², 9.01 mF cm⁻², and 4.09 mF cm⁻², respectively. Overall, the MAMNSPs electrode shows 1.9 times capacitance of that for MANSPs. Meanwhile, the capacitance of the MAMNSPs electrode is 4.26 times of that for the MAPL electrode, which is a logic result of double side conformal electrodeposition of MnO₂. With the same mass loading, such superior performance can only be ascribed to the enhanced surface area for NSPs electrodes, and larger surface area for the same mass loading leads to thinner layer MnO₂ coating on NSPs, which can potentially shorten distance for both electron and ion diffusion, leading to better faradic surface charge storage. To further confirm this hypothesis, different electrodeposition time (5 s – 120 s) of MnO₂ was conducted on free-standing Au NSPs, as shown in Figure S6. CV performance of MAMNSPs electrode show that electrodeposition time of 45 s has the best performance (SI, Figure S7a and b). Therefore, 45 s deposition time was used for all MAMNSPs electrodes and that led to 40 nm thick MnO₂ on NSPs. This result clearly indicates that excessive thickness of MnO₂ leads to the hindered ion and charge transport which in turn compromises the overall electrochemical capacitance and this is consistent with previous report.¹⁵ Meanwhile, Figure 3d and SI, Figure S8a show CV curves of a MAMNSPs electrode at different scan rate after 45 s electrodeposition. Obviously, these CV curves still retain symmetrically rectangular shape without any distortion with the increasing scan rate from 10 mV s⁻¹ to 500 mV s⁻¹, demonstrating highly reversible redox reaction. GCD with different current density (0.3 mA cm⁻² - 5 mA cm⁻²) was also plotted in SI, Figure S8b. The highly symmetric curve for charge and discharge process indicates the excellent capacitive behavior of MAMNSPs electrode. According to Figure 3e, the specific and areal capacitance are 581.3 F g⁻¹ and 17.44 mF cm⁻² at the scan rate of 10 mV s⁻¹ and 298.6 F g⁻¹ and 8.96 mF cm⁻² at the scan rate of 500 mV s⁻¹. The excellent rate capability further demonstrates the advantages of as-fabricated electrode here.

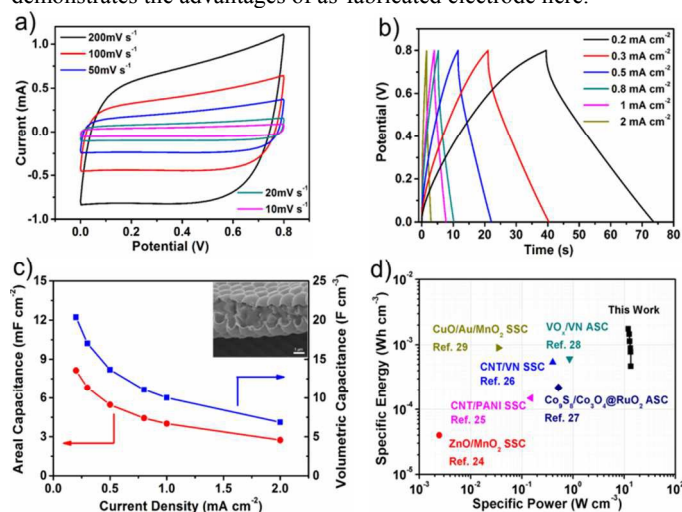


Figure 4 a) CV curves of symmetric supercapacitor at different scan rates (10 mV s⁻¹ - 200 mV s⁻¹). b) GCD curves of supercapacitor device with different current density (0.2 mA cm⁻² - 2 mA cm⁻²). c) Areal capacitance and volumetric capacitance of the device as a function of different discharge current density and SEM (insert) shows the device thickness is around 4 μm. d) Ragone plot shows the specific energy and specific power of the device.

To further explore the practical merit of the MAMNSPs electrodes, all-solid-state symmetric supercapacitor was fabricated using the following process. Two pieces of Au NSPs films were transferred onto two pieces of regular Xerox printing paper followed by electrodeposition of MnO_2 to achieve MAMNSPs electrodes. Thereafter, they were uniformly coated with H_3PO_4 /poly (vinyl alcohol) (PVA) gel electrolyte and assembled together. The all-solid-state device was finally achieved by drying up the excess water in the gel electrolyte. Electrochemical performance of the device was analyzed by CV measurements at the scan rate from 10 mV s^{-1} to 200 mV s^{-1} as shown in Figure 4a. GCD with different current density from 0.2 mA cm^{-2} to 2 mA cm^{-2} were also plotted in Figure 4b. Note that the nice rectangular shape of CV curve and liner voltage-time profiles achieved from GCD curve demonstrate a good capacitive performance. As shown in Figure 4c, the areal capacitance and volumetric capacitance for the device is 8.14 mF cm^{-2} and 20.35 F cm^{-3} at the current density of 0.2 mA cm^{-2} . Since the volumetric capacitance and energy density are size-dependent, we have successfully decreased the volume of the device. The device SEM cross section image is inserted in Figure 4c, it is composed of two pieces of as-prepared electrodes ($1.5 \mu\text{m}$ for each) and the gel electrolyte, and the total thickness of the device is as thin as $4 \mu\text{m}$ without counting the thickness of paper substrate. The specific energy and specific power based on the volume of the device were calculated according to the following formula:

$$E = C_V(\Delta E)^2/2 \quad (4)$$

$$P = (\Delta E)^2/4RV \quad (5)$$

$$R = U_{\text{drop}}/2I \quad (6)$$

$$C_V = I/(-dU/dt) \quad (7)$$

where E and P are specific energy and specific power calculated based on the volume. C_V is the volumetric capacitance of the device, ΔE is the operating voltage window excluding the voltage drop (U_{drop}), R is the internal resistance of the device, V is the volume of the device, I is the constant discharge current, and dU/dt is the slope of the discharge curve. The Ragone plot showing the specific energy with respect to specific power calculated based on the volume of the device can be seen in Figure 4d. The highest specific energy of the as-fabricated device is $1.75 \times 10^{-3} \text{ Wh cm}^{-3}$ at a specific power of 12.01 W cm^{-3} , which is among the highest when compared with the previously reported values.³⁰⁻³⁵

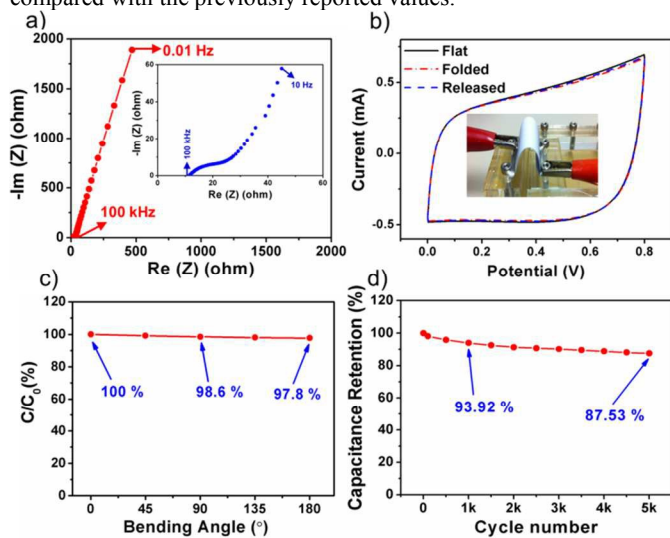


Figure 5 a) Nyquist plot of the symmetric supercapacitor device. b) CV measurements at the scan rate of 100 mV s^{-1} when the device is folded and released. c) Device bending test under different angles. d) Cycling performance of device during 5000 cycles at the scan rate of 100 mV s^{-1} .

To further test the electrochemical performance of the device, electrochemical impedance spectroscopy (EIS) measurements were conducted in the frequency range from 100 kHz to 0.01 Hz and the result is shown in Figure 5a. Equivalent series resistance (ESR) as low as 11Ω can be obtained at the x intercept of the Nyquist plot. The small radius of the semicircle in the high frequency range reflects the small charge-transfer resistance and the straight line nearly paralleled to the imaginary axis at low frequency demonstrates the ideal capacitive behavior.³⁶ For practical operation of a flexible supercapacitor device, bending performance and cyclic stability are two important characteristics.³⁷⁻⁴² In this regard, CV measurements when a device is folded and released were conducted at the scan rate of 100 mV s^{-1} . As shown in Figure 5b, there is no apparent change of the CV curve and the calculated capacitance difference is only 1.3 % after being released. Figure 5c shows the capacitance under different bending angles (0° , 45° , 90° , 135° , 180°), confirming the marginal performance change with bending of the device. Figure 5d shows the capacitance retention after multiple cycles of CV scan at a rate of 100 mV s^{-1} with voltage test window 0 to 0.8 V. It can be seen that the capacitance still maintains nearly 94 % of its initial value after 1,000 cycles and 88 % after 5,000 cycles, which shows an excellent cycle life.

Conclusions

Herein, we report the ordered freestanding 3-D MAMNSPs electrodes fabricated on 3-D Au NSPs architecture. The ultra-thin Au NSPs films have excellent transferability and flexibility. The large surface area of this unique structure leads remarkable enhancement in electrochemical performance, 1.9 and 4.26 times capacitance as compared with MANSPs and MAPL electrodes, respectively. Moreover, the all-solid-state symmetric supercapacitors based on MAMNSPs electrodes fabricated in this work showed that the devices have high volumetric capacitance of 20.35 F cm^{-3} and specific energy of $1.75 \times 10^{-3} \text{ Wh cm}^{-3}$. In addition, marginal change of the capacitance upon bending measurement and attractive cyclic stability showed that the supercapacitor devices are highly flexible and reliable. With virtue of simple fabrication procedures and enhanced electrochemical performance, such 3-D structures have highly promising potency for portable and flexible energy storage systems for a wide range of practical applications.

Experimental section

Preparation of aluminum NSPs template. Aluminum foil with the thickness of 0.25 mm and area of $3 \text{ cm} \times 2 \text{ cm}$ was prepared by cutting, followed by electrochemically cleaning under 15 V constant voltage for 2 mins. After that, $1.5 \text{ cm} \times 1.5 \text{ cm}$ silicon stamps with ordered square nanopillars with the height of $0.2 \mu\text{m}$ and controllable pitches including $0.5 \mu\text{m}$, $1 \mu\text{m}$, $1.2 \mu\text{m}$, and $1.5 \mu\text{m}$ were utilized as imprinting molds to produce a nanoindentation array on the surface of as-prepared aluminum foil. Afterwards, the aluminum NSPs template with different pitches were achieved by one-step anodization and wet etching process with proper control of solution concentration, temperature, time and direct current (DC) voltage.

Fabrication of freestanding Au NSPs film. Aluminum NSPs with $1.5 \mu\text{m}$ pitch was firstly converted into alumina NSPs via low voltage anodization process (20 V in $3.4 \text{ wt} \% \text{ H}_2\text{SO}_4$ for 16 hrs), which works as the etching layer. Thereafter, 100 nm Au was uniformly coated onto alumina NSPs with the method of sputtering deposition, followed by etching away the template

in the acidic solution composed of 1.8 wt % H_2CrO_4 and 6 wt % H_3PO_4 with the temperature of 70 °C for 5 hrs. The etching solution was then neutralized by DI water after the Au NSPs film detached from the template and floated up. Arbitrary substrates such as Xerox printing paper, PC, etc. could be immersed into solution and placed below the film. Ultimately, the as-fabricated film could lie on the target substrates after draining away the solution by syringe pump.

Fabrication of MAMNSPs electrodes. Au NSPs film was transferred onto Xerox paper followed by an anode deposition process. Different amount of MnO_2 was deposited by precisely control the time from 5 s to 120 s with the constant current density of 0.25 mA cm^{-2} at room temperature. The deposition solution consists of 0.01 M manganese acetate (MnAc_2), 98 % purity and 0.02 M ammonium acetate (NH_4Ac), 99 % purity dissolved into 90 % DI water and 10 % dimethyl sulfoxide (DMSO).

Assembling of all-solid-state symmetric supercapacitors. 12 g PVA and 12 g 85 wt % H_3PO_4 were dissolved into 120 ml DI water. After that, the solution was vigorously stirred at 85 °C until it became clear. Then, the solution was cooled down to the room temperature and worked as gel electrolyte. Two pieces of MAMNSPs electrodes were fabricated beforehand, and one of the as-proposed electrodes was immersed into H_3PO_4 /poly (vinyl alcohol) (PVA) gel electrolyte for 5 mins. Due to the porous nature of the Xerox printing paper, the gel electrolyte could penetrate through the substrate and thus, the electrode could be double-side coated with gel electrolyte. Afterwards, to achieve uniform distribution of the gel electrolyte, spin coating was performed at the rotate speed of 4000 r min^{-1} for 2 mins. Thereafter, the as-proposed electrode was placed onto the hotplate with the temperature of 60 °C for 1 hr to vaporize the excess water. A similar way but without drying process was used for another MAMNSPs electrode, and after spin coated, the electrode was directly placed onto the previous one to finish assembling the final device.

Characterization of samples

Various analytical techniques were utilized to characterize the as-built nanostructured electrode. Morphologies were characterized using field-emission scanning electron microscopy (JSM-7100F, Japan). Chemical compositions were studied by X-ray photoelectron spectroscopy (PHI 5600, USA). CV, GCD and EIS measurements based on both two-electrode and three-electrode configuration were performed on an electrochemical workstation (CHI 660E, China). CV was carried out at different scan rates of 10, 20, 50, 100, 200 and 500 mV s^{-1} . GCD was measured at 0.2, 0.3, 0.5, 0.8, 1, 2, 5 mA cm^{-2} . EIS was measured with the frequency range from 100 kHz to 0.01 Hz with potential amplitude of 10 mV.

Acknowledgements

This work was supported by General Research Fund (612113) from the Hong Kong Research Grant Council and partially supported by Hong Kong Innovation and Technology Fund (ITS/117/13) from the Innovation and Technology Commission. The authors also thank Dr. S. Y. Gan from Chang Chun Institute of Applied Chemistry, Chinese Academy of Sciences for his helpful discussion.

Notes and references

- ^a Department of Electronic and Computer Engineering, Hong Kong University of Science and Technology, Clear Water Bay, Kowloon, Hong Kong, China SAR.
^b Department of Applied Physics, The Hong Kong Polytechnic University, Hung Hom, Hong Kong, China SAR.
^c Department of Mechanical Engineering, The Hong Kong Polytechnic University, Hung Hom, Hong Kong, China SAR

*Corresponding Author: Zhiyong Fan; E-mail: eezfan@ust.hk

† Electronic Supplementary Information (ESI) available: Photographs of mechanical robustness test of Au NSPs film and schematic illustration of point contacts among NSPs are shown in Figure S1. Optical image of free-standing Au NSPs film and Si stamps with the area of $1.5 \text{ cm} \times 1.5 \text{ cm}$ are shown in Figure S2. SEM images of Au NSPs with the pitches of 0.5 μm , 1 μm , 1.2 μm and 1.5 μm are shown in Figure S3. Schematic illustration of surface area calculation and surface enhancement results are plotted in Figure S4. XPS and XRD of the materials are shown in Figure S5. SEM images of different electrodeposition time are shown in Figure S6. CV curves after different electrodeposition time (5 – 120 s) and related areal capacitance are shown in Figure S7. CV ($300 - 500 \text{ mV s}^{-1}$) and GCD ($0.3 - 5 \text{ mA cm}^{-2}$) curves of MAMNSPs electrode after electrodeposition of 45 s are shown in Figure S8. See DOI: 10.1039/b000000x/

1 Z. Y. Fan, D. Dutta, C. J. Chien, H. Y. Chen, E. C. Brown, P. C. Chang and J. G. Lu, *Appl. Phys. Lett.*, 2006, **89**, 213110-213112.

2 Z. Y. Fan, J. C. Ho, Z. A. Jacobson, H. Razavi and A. Javey, *Proc. Natl. Acad. Sci. U. S. A.*, 2008, **105**, 11066-11070 (DOI:10.1073/pnas.0801994105 ER).

3 J. Li, Y. Qiu, Z. Wei, Q. Lin, Q. Zhang, K. Yan, H. Chen, S. Xiao, Z. Fan and S. Yang, *Energy & Environmental Science*, 2014, **7**, 3651-3658.

4 Y. Qiu, S. Leung, Q. Zhang, B. Hua, Q. Lin, Z. Wei, K. Tsui, Y. Zhang, S. Yang and Z. Fan, *Nano Lett.*, 2014, **14**, 2123-2139.

5 S. Leung, L. Gu, Q. Zhang, K. Tsui, J. Shieh, C. Shen, T. Hsiao, C. Hsu, L. Lu, D. Li, Q. Lin and Z. Fan, *Sci. Rep.*, 2014, **4**, 4243.

6 Q. Lin, S. Leung, L. Lu, X. Chen, Z. Chen, H. Tang, W. Su, D. Li and Z. Fan, *ACS Nano*, 2014, **8**, 6484-6490.

7 Y. Qiu, Y. Zhao, X. Yang, W. Li, Z. Wei, J. Xiao, S. Leung, Q. Lin, H. Wu and Y. Zhang, *Nanoscale*, 2014, **6**, 3626-3631.

8 Z. Yu, B. Duong, D. Abbitt and J. Thomas, *Adv Mater*, 2013, .

9 D. N. Futaba, K. Hata, T. Yamada, T. Hiraoka, Y. Hayamizu, Y. Kakudate, O. Tanaike, H. Hatori, M. Yumura and S. Iijima, *Nature materials*, 2006, **5**, 987-994.

10 C. K. Chan, H. L. Peng, G. Liu, K. McIlwrath, X. F. Zhang, R. A. Huggins and Y. Cui, *Nature Nanotechnology*, 2008, **3**, 31-35 (DOI:10.1038/nnano.2007.411 ER).

11 Y. Gogotsi, *Nature*, 2014, **509**, 568-570.

12 J. R. Miller and P. Simon, *Science Magazine*, 2008, **321**, 651-652.

13 D. Pech, M. Brunet, H. Durou, P. Huang, V. Mochalin, Y. Gogotsi, P. Taberna and P. Simon, *Nature nanotechnology*, 2010, **5**, 651-654.

- 14 P. Simon and Y. Gogotsi, *Nature materials*, 2008, **7**, 845-854.
- 15 S. Chabi, C. Peng, D. Hu and Y. Zhu, *Adv Mater*, 2014, **26**, 2440-2445.
- 16 Z. Su, C. Yang, B. Xie, Z. Lin, Z. Zhang, J. Liu, B. Li, F. Kang and C. Wong, *Energy & Environmental Science*, 2014, .
- 17 B. Duong, Z. Yu, P. Gangopadhyay, S. Seraphin, N. Peyghambarian and J. Thomas, *Advanced Materials Interfaces*, 2014, **1**.
- 18 U. N. Maiti, J. Lim, K. E. Lee, W. J. Lee and S. O. Kim, *Adv Mater*, 2014, **26**, 615-619.
- 19 Z. Yu, C. Li, D. Abbitt and J. Thomas, *Journal of Materials Chemistry A*, 2014, .
- 20 Z. Yu, L. Tetard, L. Zhai and J. Thomas, *Energy & Environmental Science*, 2015, .
- 21 H. Zhao, C. Wang, R. Vellacheri, M. Zhou, Y. Xu, Q. Fu, M. Wu, F. Grote and Y. Lei, *Adv Mater*, 2014, **26**, 7654-7659.
- 22 R. Yi, S. Chen, J. Song, M. L. Gordin, A. Manivannan and D. Wang, *Advanced Functional Materials*, 2014, **24**, 7433-7439.
- 23 X. Wang, X. Lu, B. Liu, D. Chen, Y. Tong and G. Shen, *Adv Mater*, 2014, **26**, 4763-4782.
- 24 X. Xia, D. Chao, Z. Fan, C. Guan, X. Cao, H. Zhang and H. J. Fan, *Nano letters*, 2014, **14**, 1651-1658.
- 25 X. Xia, Y. Zhang, Z. Fan, D. Chao, Q. Xiong, J. Tu, H. Zhang and H. J. Fan, *Advanced Energy Materials*, 2014, .
- 26 M. F. El-Kady, V. Strong, S. Dubin and R. B. Kaner, *Science*, 2012, **335**, 1326-1330 (DOI:10.1126/science.1216744 [doi]).
- 27 Z. Su, C. Yang, C. Xu, H. Wu, Z. Zhang, T. Liu, C. Zhang, Q. Yang, B. Li and F. Kang, *Journal of Materials Chemistry A*, 2013, **1**, 12432-12440.
- 28 S. Zhu, Y. Gao, B. Hu, J. Li, J. Su, Z. Fan and J. Zhou, *Nanotechnology*, 2013, **24**, 335202.
- 29 S. Leung, K. Tsui, Q. Lin, H. Huang, L. Lu, J. Shieh, C. Shen, C. Hsu, Q. Zhang and D. Li, *Energy Environ. Sci.*, 2014, **7**, 3611-3616.
- 30 X. Lu, M. Yu, T. Zhai, G. Wang, S. Xie, T. Liu, C. Liang, Y. Tong and Y. Li, *Nano letters*, 2013, **13**, 2628-2633.
- 31 X. Xiao, X. Peng, H. Jin, T. Li, C. Zhang, B. Gao, B. Hu, K. Huo and J. Zhou, *Adv Mater*, 2013, **25**, 5091-5097.
- 32 J. Xu, Q. Wang, X. Wang, Q. Xiang, B. Liang, D. Chen and G. Shen, *ACS nano*, 2013, **7**, 5453-5462.
- 33 P. Yang, X. Xiao, Y. Li, Y. Ding, P. Qiang, X. Tan, W. Mai, Z. Lin, W. Wu and T. Li, *ACS nano*, 2013, **7**, 2617-2626.
- 34 M. Yu, Y. Zhang, Y. Zeng, M. Balogun, K. Mai, Z. Zhang, X. Lu and Y. Tong, *Adv Mater*, 2014, .
- 35 Z. Yu and J. Thomas, *Adv Mater*, 2014, .
- 36 W. Chen, R. Rakhi, L. Hu, X. Xie, Y. Cui and H. Alshareef, *Nano letters*, 2011, **11**, 5165-5172.
- 37 X. Xiao, T. Li, P. Yang, Y. Gao, H. Jin, W. Ni, W. Zhan, X. Zhang, Y. Cao and J. Zhong, *Acs Nano*, 2012, **6**, 9200-9206.
- 38 L. Yuan, X. Lu, X. Xiao, T. Zhai, J. Dai, F. Zhang, B. Hu, X. Wang, L. Gong and J. Chen, *Acs Nano*, 2011, **6**, 656-661.
- 39 L. Chen, Z. Yu, J. Wang, Q. Li, Z. Tan, Y. Zhu and S. Yu, *Nano Energy*, 2015, **11**, 119-128.
- 40 L. Huang, C. Li and G. Shi, *Journal of Materials Chemistry A*, 2014, **2**, 968-974.
- 41 L. Wu, R. Li, J. Guo, C. Zhou, W. Zhang, C. Wang, Y. Huang, Y. Li and J. Liu, *AIP Advances*, 2013, **3**, 082129.
- 42 C. Meng, C. Liu, L. Chen, C. Hu and S. Fan, *Nano letters*, 2010, **10**, 4025-4031.

The table of contents entry

Highly Flexible and Transferable Supercapacitors with Ordered Three-dimensional MnO₂/Au/MnO₂ Nanospikes Arrays

Free-standing Au NSPs film is fabricated by simply wet etching process. The ultra-thin Au NSPs film has excellent transferability and remains highly ordered upon bending. Supercapacitors fabricated based on MnO₂/Au/MnO₂ NSPs (MAMNSPs) electrodes show remarkable enhancement in electrochemical performance such as volumetric capacitance and energy density. Such unique structures demonstrate promising application for portable and flexible energy storage systems.

